Eur. Phys. J. Special Topics **223**, 455–467 (2014)

DOI: 10.1140/epjst/e2014-02102-6

THE EUROPEAN PHYSICAL JOURNAL SPECIAL TOPICS

Review

Characterization of local structures with bond-order parameters and graphs of the nearest neighbors, a comparison

U. Gasser[1,a], F. Ziese[2], and G. Maret[2]

[1] Laboratory for Neutron Scattering, Paul Scherrer Institut, 5232 Villigen, Switzerland
[2] Physics Department, University of Konstanz, D-78457 Konstanz, Germany

Received 13 December 2013 / Received in final form 10 January 2014
Published online XX February 2014

Abstract. We compare two methods for the characterization of local order in samples undergoing crystal nucleation and growth. Particles with a crystal-like surrounding need to be identified to follow the nucleation process. Both methods are based on the knowledge of the particle positions in a small volume of the sample. (i) Local bond-order parameters are used to quantify the orientation of the nearest neighbors of a particle, while (ii) the graph method determines the topological arrangement of the nearest neighbors and the bonds between them. Both methods are used to detect crystal-like particles and crystal nuclei in a supercooled fluid surrounding and to determine the structure of small crystal nuclei. The properties of these nuclei are of great interest for a deeper understanding of crystal nucleation, and they can be studied in detail in colloidal model systems that allow to follow the evolution of the nuclei with single particle resolution.

1 Introduction

Crystal nucleation, the first order phase transition from a supercooled fluid to a crystal, continues to be a topic in condensed matter research, as a quantitative understanding of the physical processes involved in crystal nucleation is still missing. This is highlighted by the fact that measured and calculated nucleation density rates, one of the key quantities of nucleation, often differ by several orders of magnitude [1,2]. According to classical nucleation theory (CNT), the nucleation process is controlled by the parameters giving the free energy barrier between the crystal and the supercooled fluid state:

$$\Delta G_{hom} = \gamma\, A - \Delta\mu\, n\, V \tag{1}$$

for homogenous nucleation with the surface tension γ, the crystal nucleus area A, the difference of the chemical potentials $\Delta\mu$, the particle number density in the crystal

[a] e-mail: urs.gasser@psi.ch

state n, and the volume V of the nucleus. The key parameters γ and $\Delta\mu$ are, however, not well known, as experiments indicate that the values for small crystal nuclei differ from those of the bulk crystal [2–4]. Therefore, studies of the nucleation process and the properties of small crystal nuclei are of high interest to obtain the key parameters of nucleation as an input for more exact theories.

Colloidal suspensions can be used as model systems for the study of small crystal nuclei. A particle size in the range from $\sim$100 nm to a few microns allows to observe crystal nuclei by scattering techniques or direct imaging with a time resolution allowing to follow the formation and evolution of the nuclei [2,3,5–10]. Using colloidal model systems, it has been revealed that the shape of precritical nuclei is rather irregular [3,4,11,12], while the surface tension suggests that a spherical shape is expected. This observation reflects estimates of γ for precritical nuclei [3] finding a surface tension smaller than that of the bulk crystal.

The observation of crystal nuclei by direct imaging methods implies that the nuclei forming at random locations due to homogenous nucleation need to be found in the environment of the supercooled fluid. Methods for the detection of these nuclei cannot rely on the procedure of crystal characterization used for bulk crystal, as the nuclei are too small to show Bragg peaks and are expected to be strongly disordered, as the majority of particles forming the nuclei are in contact with the surrounding fluid. The most widely used method for the detection of crystal nuclei and the characterization of its structure is that of bond-order parameters that were originally introduced to characterize the local structures in disordered materials [13] but have been used for the identification of crystal-like local structures in simulations [4,14–16] and direct imaging experiments [3,11,12,17,18]. This method is based on the quantification of the spatial arrangement of nearest neighbor particles around a central particle. These values are determined for all particles of interest and are compared to identify structural changes. Bond-order parameters are based on spherical harmonic functions and, therefore, there are many types of them and they can be chosen to fit the properties of the material of interest. Also, several variants and combinations of bond-order parameters have been proposed for the identification of crystal nuclei [19]. An alternative method is given by the analysis of graphs corresponding to nearest neighbors around a central particle and the bond between them, a topological method. As the bond-order parameters, the graph method has been introduced to characterize the local structures of disordered materials [20].

Here, we present a comparison of the two methods mentioned above and compare them with confocal microscopy data of colloidal suspensions undergoing crystal nucleation. We first introduce both methods and then focus on their applicability to identify particles with crystal-like surrounding in an undercooled fluid and to characterize the local structures found in crystal nuclei of precritical size.

2 Experimental

To follow the process of crystal nucleation experimentally, we use colloidal poly(methyl methacrylate) (PMMA) particles with a diameter $d = (1.90 \pm 0.05)\,\mu$m and a polydispersity of 0.067 ± 0.005 as determined by dynamic light scattering and a CONTIN analysis [21]. The particles are suspended in a refractive index and density matching solvent given by a mixture of decahydronaphtalene (decalin) and cycloheptylbromide (CHB). The solvent is mixed such that no particle sedimentation is found after centrifuging for 16 hours at 2500 rotations per minute. With this mixture, the refractive index of the PMMA particles (≈ 1.497) is nearly matched, and particles can be imaged at a depth of 100 μm in the sample using confocal microscopy.

The PMMA particles are found to carry a relatively small charge of about 380 elementary charges and to interact like hard spheres with a Yukawa interaction [22]. The interaction is given by

$$\frac{V(r)}{k_B T} = \begin{cases} K \frac{\exp(-\kappa[r-d])}{r/d}, & r > d \\ \infty, & r < d \end{cases}, \tag{2}$$

where K is the dimensionless contact value and κd the dimensionless screening parameter. From a comparison with experimentally determined radial distribution functions, $g(r)$, using Ornstein-Zernike calculations with the hypernetted-chain approximation [23] we find the values $K = 42 \pm 8$ and $\kappa d = 5.75 \pm 0.5$ [12]. The particles are dyed with fluoresceine to make them visible with confocal microscopy. From microcopy measurements at ambient temperature with samples at various particle volume fractions, we have determined the freezing point to be $\phi_f = 0.16 \pm 0.01$ [12]. This is in good agreement with the simulation study of the phase behavior of hard-sphere-Yukawa particles given in Ref. [22], which also shows that the equilibrium crystal structure is fcc.

To obtain reference data for our particles with fcc or hcp structure, we have carried out Monte-Carlo simulations of ≈ 8800 particles with the hard-core-Yukawa interaction given above and in a box with periodic boundary conditions. The simulations were started with the perfect fcc and hcp structures and $2 \cdot 10^4$ Monte-Carlo moves were carried out for each particle. This data is used to obtain reference data for local bond-order parameters and the graphs and shortest-path rings, as described in the following.

3 Results and discussion

3.1 Nearest neighbors

Both the local bond-order and the ring method rely on the knowledge of the nearest neighbors of each particle. This can be obtained in two ways: Using a cut-off distance, all particles with a distance smaller than the cut-off from a central particle are identified as nearest neighbors. Alternatively, the Voronoi construction [24,25] can be used to find neighboring particles even in an environment with anisotropic average particle arrangement. Both methods have their advantages and disadvantages. For the study of crystal nucleation in nearly hard spheres, the fcc and hcp crystal lattices are of primary interest. In both lattices, a particle has 12 nearest neighbors, which is roughly the same as in the hard-sphere fluid. The distance for which 12 nearest neighbors are obtained on average can be determined from the radial distribution function, $g(r)$, using the condition $4\pi n \int_0^{R_{12}} dr g(r) = 12$, where n is the average number density of the particles. When R_{12} is used as the nearest neighbor cut-off, one is implicitly tuning the analysis for the detection of crystal structures with 12 nearest neighbors.

The Voronoi construction does not rely on a cut-off distance: All the neighbors that are necessary to define the polyhedron containing all points that are closer to a central particle than to any other particle are identified as nearest neighbors. The Voronoi polyhedron consists of faces that are part of the plane intersecting the bond between the central and a nearest neighbor particle; each nearest neighbor is associated to a face of the Voronoi polyhedron. In general, three faces of the polyhedron touch at a vertex. However, for the fcc and hcp lattices, four faces touch at some of the vertices, which implies that these vertices are degenerate in the

sense that small errors or deviations in the particle positions will generate additional faces in the polyhedron such that three faces touch at each vertex [26]. This implies that the number of nearest neighbors in the fcc and hcp lattices identified using the Voronoi construction varies from particle to particle [27]. This problem can, however, be solved by giving each bond determined using the Voronoi construction a weight given by the area of the corresponding Voronoi face, as explained in detail in Ref. [28]. This allows to suppress the disturbing influence of second nearest neighbors (small Voronoi faces), while the nearest neighbors (large Voronoi faces) carry the dominating weights. In the following, we determine nearest neighbors with a simple cut-off distance chosen such that we have 12 nearest neighbors on average.

3.2 Local bond-order parameter

Local bond-order parameters have been introduced to quantify the local structures found in disordered materials [13]. The underlying idea is to express the arrangement of the nearest neighbors using spherical harmonic functions, Y_{lm}. The bond-order parameter $q_{lm}(i)$ of a particle i is defined as

$$q_{lm}(i) = \frac{1}{N(i)} \sum_{j=1}^{N(i)} Y_{lm}(\hat{r}_{ij}) \tag{3}$$

with $N(i)$ the number of nearest neighbors particles. The number of lobes of the functions Y_{lm} is given by l. The higher this number, the larger the number of specific arrangements of the neighbors that can be captured. The symmetry of the spherical harmonics is also given by l. $l = 6$ is the natural value for the detection of fcc- and hcp-like structures, as the hexagonal planes in these crystal lattices have six-fold symmetry.

Particles with a crystal-like surrounding can be identified by comparing the values of $q_{6m}(i)$ with those of the nearest neighbors. This is done by computing the inner product

$$s_6(i,j) = \sum_{m=-l}^{l} \hat{q}_{6m}(i)\, \hat{q}^*_{6m}(j), \tag{4}$$

where we use the normalized bond-order parameter $\hat{q}_{lm} = q_{lm}/\sqrt{\sum_m q_{lm} q^*_{lm}}$. The "bond" between two neighboring particles i and j is called a crystal-like bond, if $s_6(i,j) > 0.5$. A particle with eight or more crystal-like bonds with its nearest neighbors is called a crystal-like particle. These two criteria allow for a good separation of fluid- and crystal-like local structures: In the supercooled fluid state, the number of crystal-like particles is low ($< 3\%$) before crystal nucleation starts and, in crystalline samples with ϕ above the melting point, the number of fluid-like particles is also low ($< 1\%$). In literature, different cut-off values for $s_6(i,j)$ and the number of crystal-like bonds can be found [4,29–31]. The range of the $s_6(i,j)$ cut-off varies from 0.5 to 0.7, and this value has to be balanced with an appropriate number of crystal-like bonds for crystal-like particles. With a cut-off of 0.7 for $s_6(i,j)$, the number of crystal-like bonds required for a crystal-like particles is usually reduced to six.

As far as the local structure of a crystal-like particle is concerned, we are interested in a measure of the structure that does not depend on the particular orientation of the bonds to the nearest neighbors as for the complex vectors q_{lm}. Therefore, rotational

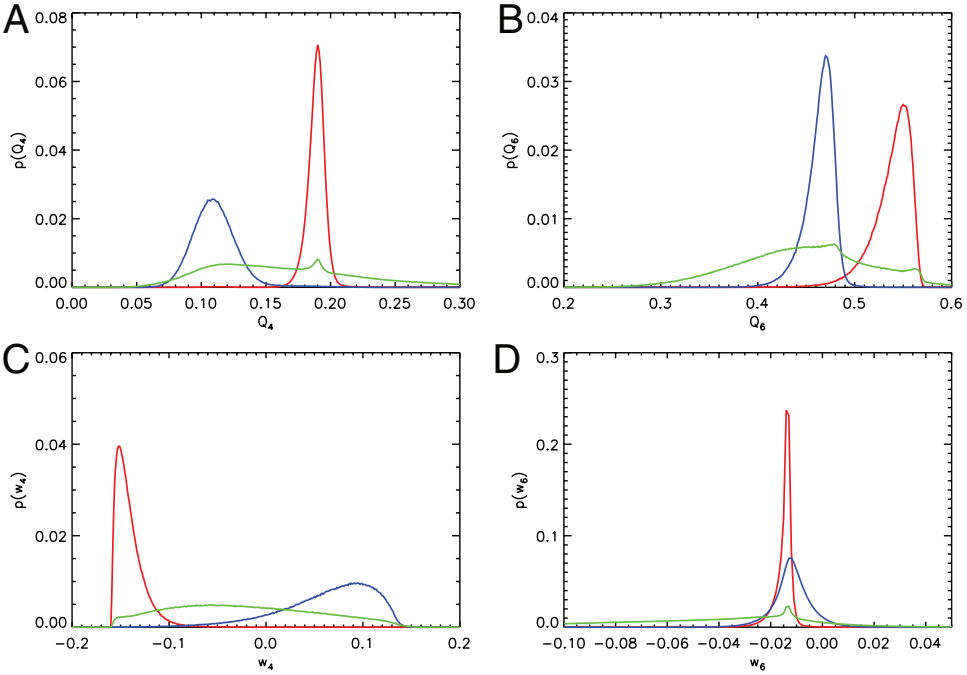

Fig. 1. Histograms of the bond-order parameters q_4, q_6, w_4, and w_6 from Monte-Carlo simulations of crystals with fcc (red) and hcp (blue) structure with $\phi = 0.28$ and a measurement of a crystallizing sample (green) also at $\phi = 0.28$.

invariants of the bond-order parameters are calculated. The second order and third order invariants

$$Q_l(i) = \left[\frac{4\pi}{2l+1} \sum_{m=-l}^{l} |q_{lm}(i)|^2 \right]^{1/2} \tag{5}$$

$$w_l(i) = \sum_{\substack{m_1,m_2,m_3 \\ m_1+m_2+m_3=0}} \begin{pmatrix} l & l & l \\ m_1 & m_2 & m_3 \end{pmatrix} \hat{q}_{lm_1}(i)\, \hat{q}_{lm_2}(i)\, \hat{q}_{lm_3}(i) \tag{6}$$

are commonly used. $\begin{pmatrix} l & l & l \\ m_1 & m_2 & m_3 \end{pmatrix}$ represents the Wigner $3j$-symbol, which is the same as the Clebsch-Gordan coefficient up to a factor. The distribution of all these values are used to differentiate between crystal structures as well as the fluid [3,12–17,32, 33]. Reference distributions that can be compared with data from simulations of various crystal or fluid structures. Figure 1 shows bond-order parameter distributions obtained from Monte Carlo distributions of hard-core-Yukawa particles at a volume fraction $\phi = 0.28$. The parameters Q_4, Q_6, and w_4 are used to distinguish between fcc and hcp. The overlap of the w_6 distributions is large and, therefore, this parameter is not used. These are compared with a measurement of a sample undergoing crystal nucleation with the same ϕ.

The bond-order parameters Q_4, Q_6, w_4, and w_6 do not allow to separate fcc-, hcp-, or fluid-like order in a unique way, as the distributions overlap to a small extent. For this reason, it has recently been discussed whether the bond-order parameters as given above are the optimum parameters for structure determination. Lechner and Dellago have used simulation data of pure structures to look for parameters allowing

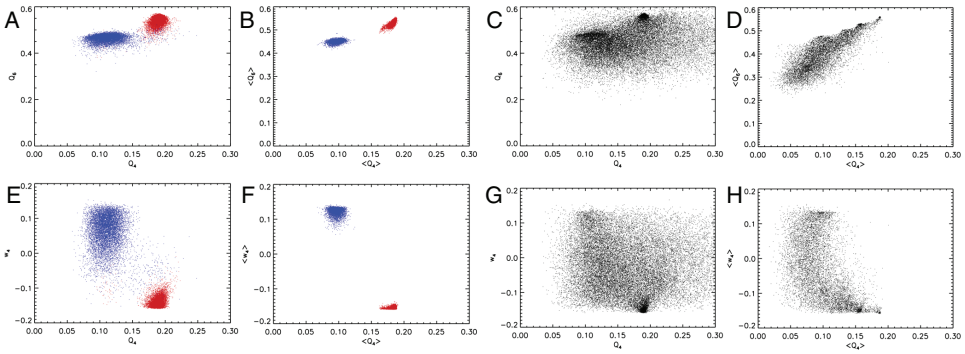

Fig. 2. Comparison of the Q_4-, Q_6-, and w_4-distributions and their averages over nearest neighbors for (A, B, E, F) simulations of fcc and hcp at $\phi = 0.28$ and for (C, D, G, H) a measurement at $\phi = 0.28$.

a clear separation of fcc and hcp in particular [19]. They have found that bond-order parameters averaged over the nearest neighbors improve the distinction of the structures:

$$q'_{lm}(i) = \frac{1}{N_i + 1} \sum_{j \in \{i, neighbors\}} q_{lm}(j), \tag{7}$$

where the sum runs over the particle i and its N_i nearest neighbors. The averaging reduces fluctuations that can lead to a clear separation of bulk structures, as shown in [19] and Fig. 2A, B, E, F. However, we are mainly interested in small crystal nuclei, i.e. crystal-like particles that are not embedded in a bulk structure but are always close to the crystal-fluid boundary. In small nuclei, the local structure changes over the distance of the nearest neighbors and most crystal-like particles have fluid-like neighbors. For this reason, the averaging over next nearest neighbors does not narrow the bond-order parameter distributions as effectively but leaves a broad distribution that still shows a large overlap, as shown in Fig. 2C, D, G, H.

3.3 Graphs of next nearest neighbor structures and shortest-path rings

As an alternative to the bond-order parameters, the local structures defined by the nearest neighbor particles of a central particle can be treated as a graph [20,27,34,35]. The neighbor particles without the central particle correspond to the vertices and the nearest-neighbor bonds between them are the edges of the graph. Graphs obtained in this way are known as simple planar graphs. They are simple, as there are (i) no edges making a loop from one vertex back to the same vertex and (ii) there is no more than one edge between two given vertices. Furthermore, the considered graphs are planar, as edges do not cross each other. This criterion is fulfilled, because the vertices of the graph form a polyhedron, which obviously has no crossing edges. When one face of this polyhedron is enlarged and the other ones are diminished, all the vertices and edges of the graph can be moved to the side that is visible for an observer. The graphs for fcc and hcp structure are shown in Fig. 3. Both have 12 vertices, 24 edges, and 14 faces (including the outer face), which fulfills the Euler criterion for polyhedra as expected:

$$V - E + F = 2, \tag{8}$$

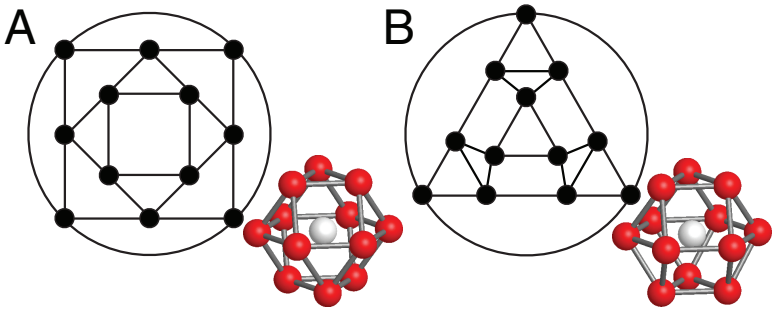

Fig. 3. Nearest neighbor graphs of the (A) fcc and (B) hcp lattice together with corresponding 3d sketches of the nearest neighbors (red) around a central particle (white). Both graphs have eight SP 3-rings, six SP 4-rings, and four SP 6-rings.

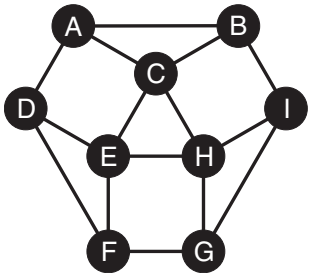

Fig. 4. A graph containing SP 3-rings, 4-rings, and 6-rings. Three 3-rings: ABC, DEF, GHI, and CEH. Three 4-rings: ACED, BCHI, and EFGH. One 6-ring: ABIGFD.

where V, E, and F give the number of vertices, edges, and faces, respectively. The two graphs give the only solutions for the case of connected, simple, planer graphs with $V = 12$, four edges per vertex, and triangular and square faces. While the Voronoi construction links the neighbors to the faces of a polyhedron, the neighbors correspond to the vertices in the graphs. As for the Voronoi construction, structural fluctuations can give rise to variations caused by missing bonds, missing particles, or additional bonds or particles. While the graphs for fcc and hcp are the only solutions for planar, simple graphs with 12 vertices and 4 edges per particle, structural fluctuations give rise to a large number of additional graphs that represent disturbed fcc or hcp structures. The most frequent of these are shown in Fig. 5. The number of disturbed structures is higher for hcp than for fcc. This is due to the lower symmetry of hcp: All edges are equivalent in fcc, while there are edges with four different surroundings for hcp. Therefore, there are more variants of deviations from the ideal structure for hcp; there are four variants of the hcp graph with one missing edge and only one for the fcc graph (Fig. 5).

As suggested by Fig. 3, the number of triangles and squares can be used to characterize a local structure. The graph method has been extended in this sense to include a generalized form of rings (circuits in the graph) [20,27,34]. A circuit is called a *shortest-path ring* (SP ring), if the path from one vertex to another along the circuit gives a shortest path between the two vertices for any pair of vertices on the circuit. The length of a path between two vertices is defined as the minimum number of edges that need to be passed to go from one vertex to the other. A few examples are given in Fig. 4. The triangles, squares, and pentagons visible in Figs. 4, 3, and 5 are

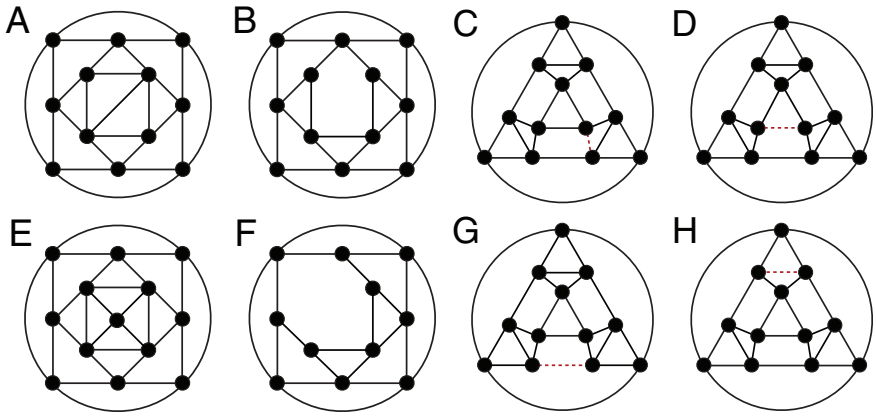

Fig. 5. Graphs with common aberrations from (A, B, E, F) the fcc graph and from (C, D, G, H) the hcp graph. Missing bonds are highlighted by dashed red lines in (C, D, G, H).

shortest-path rings, as there are no shortcuts, even taking the vertices into account that are given by the central particle or other neighboring particles. In addition, a modified definition is used for SP rings of six particles [27,34]. A *modified SP 6-ring* is a SP ring for which the central particle of the considered nearest neighbors is neglected. The central particle would always be a short cut of length two between any pair of nearest neighbors and, therefore, excludes the existence of SP 6-rings as defined above. We simply refer to the modified SP 6-rings as SP 6-rings in the following. The SP 6-rings allow to identify hexagonal planes in structures such as fcc or hcp and, therefore, are of interest for characterizing local structures relevant for crystal nucleation. Furthermore, shortest path rings give a natural way to characterize local structures [20,27] in the sense that the histogram of SP rings usually gives a peak that is characteristic for the structure. Other ring definitions do not give as clear histograms and, therefore, are not as useful for structure characterization as the SP rings [20].

In contrast to the local bond-order parameters, the graph and SP ring methods are purely topological, once the nearest neighbors (vertices) and the bonds between them (edges) are defined. Therefore, they are complementary to the bond-order parameters in the sense that the regularity of the nearest-neighbor orientation is not as important but they focus on the general arrangement of the nearest neighbors and on the bonds between them.

As the graphs of the nearest neighbors, the shortest-path rings found for the nearest neighbors of the particles can be used to characterize local structures. We take SP rings of 3, 4, 5, and 6 particles into account and, in addition, characterize the SP rings by counting their neighboring SP rings. Two SP rings are considered to be neighbors, if they share one or more edges in the graph. E.g., the fcc and hcp graphs in Fig. 3 both have eight SP 3-rings, six SP 4-rings, and four SP 6-rings. But they differ in terms of the neighboring rings: For fcc, all SP 4-rings are surrounded by 3-rings and all SP 3-ring are surrounded by three SP 4-rings, while for hcp SP 4-rings are surrounded by three SP 3-rings and a SP 4-ring and the SP 3-ring are neighboring two SP 4-rings and one SP 3-ring. In contrast to a graph, the SP-rings do not give a non-ambiguous descriptions of a local structure. I.e., there are non-equivalent graphs having the same number of SP rings with the same neighbor properties. But the SP rings capture characteristic structural properties that are of interest to follow crystal

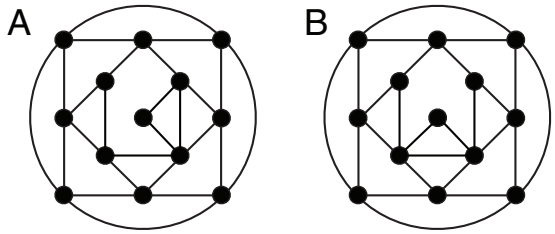

Fig. 6. Non-equivalent graphs with 13 vertices, eight SP 3-rings, five SP 4-rings, one SP 5-ring, and three SP 6-rings. A and B are equivalent in terms of SP rings.

Table 1. Number of graph structures found in Monte-Carlo simulations with ≈ 8800 particles with fcc and hcp structure at several volume fractions, ϕ. $N_{undet.}$ gives the number of undetermined crystal structures that meet neither the criteria for fcc- nor for hcp-like particles.

ϕ	0.20	0.240	0.28	0.31
N_{fcc}	5438	909	123	126
N_{hcp}	9895	2917	500	427
$N_{undet.}$	1493	137	6	4
N_{total}	16826	3963	629	557

nucleation and growth. That the SP-rings do not give non-ambiguous descriptions of the structure, is illustrated in Fig. 6. E.g. additional particles that are connected by only one bond to the other nearest neighbors are not captured by the SP-rings.

3.4 Graphs and SP ring structures from simulations

In analogy to the bond-order parameters, one can collect the different graphs and SP rings that appear in simulations of the bulk structures of interest to characterize the graphs and SP rings found in a measurement. To collect a large number of graphs, simulations are done at $\phi = 0.2$ close to the freezing point, $\phi_f \approx 0.16$, to obtain a crystal with large structural fluctuations. In addition, simulations are also done at the volume fraction of the measurement for a direct comparison, $\phi = 0.28$ in our example. The numbers of non-equivalent graph structures found in these simulations are given in Table 1; the number strongly depend on volume fraction. To collect all the non-equivalent graphs from the simulations, the graphs are represented as adjacency matrices. For a graph with N vertices, the adjacency matrix, A, has dimension $N \cdot N$, and the vertices are numbered to assign the element A_{ij} to a pair of vertices (i, j). The adjacency matrix serves to compare given graphs with adjacency matrices A_1 and A_2, as the invariants of these matrices can be compared (determinant and eigenvalues; the trace is always equal to zero). Two graphs with equal invariants can be further compared by trying to transform A_1 into A_2 using a change of basis given by the eigenvectors of both A_1 and A_2. This allows to find all equivalent graphs. For each type of graph, we determine its frequency of occurrence when we collect the non-equivalent types. With this frequency data, we assign each graph to either fcc or hcp depending of the occurrence in fcc and hcp simulations. If the occurrence in one structure is higher by at least a factor of ten than in the other, we assign a graph to the more frequent structure. If this inequality is not fulfilled, the graph is marked to represent an undefined crystal structure. The factor of ten is found to

Table 2. Percentage of crystal-like particles identified with the graph method and the bond-order method for a measurement at $\phi = 0.28$. For the graph method, the percentages of fcc-, hcp-, and undetermined crystal-like particles are given as well. Data is given for early times of the measurement during when nucleation is observed and later times where larger nuclei are found to grow.

	$\frac{N_c^X}{N}$ (%)	$\frac{N_{c\,fcc}^X}{N}$ (%)	$\frac{N_{c\,hcp}^X}{N}$ (%)	$N_c^{agreement}/N_c^X$
graphs (early)	10.2	3.1	6.6	62
bond-order (early)	12.3			51
graphs (late)	22.8	11.6	10.0	88
bond-order (late)	30.6			65

give a clear separation of fcc and hcp with a fraction of undetermined structures $N_{undet.}/N_{total} \lesssim 0.01$ for $\phi = 0.28$, as shown in Table 1. This ratio, however, strongly depends on ϕ.

3.5 Comparison with measurement

3.5.1 Comparison of crystal-like particles

The local structures from simulations are characterized by the graphs or the SP rings and are compared with the local structures found in confocal microscopy data. Simulations and measurement have the same volume fraction ($\phi = 0.28$). Crystal-like particles are determined using both methods, and crystal nuclei are found by assigning all crystal-like particles that are connected by a crystal-like bond to the same nucleus. The graph method is found to be somewhat more restrictive. For small precritical nuclei (early times in Table 2), we find the ratio of crystal-like particles, N_c, identified with the two methods to be $N_c^{graph}/N_c^{q_6} \approx 0.83$. For critical and postcritical nuclei (late times), the ratio is smaller with $N_c^{graph}/N_c^{q_6} \approx 0.74$. Given the fact that the methods do not focus on the same details of the local structures, their agreement is good. The ratio of particles that are found to be crystal-like with both methods, $N_c^{agreement}/N_c^X$, where $X \in \{graph, q_6\}$, are given in Table 2.

Although the equilibrium structure is known to be fcc, a larger number of hcp-like local structures is found in small precritical crystal nuclei, as shown in Table 2. At later times, when nuclei have reached critical and postcritical size, the number of fcc- and hcp-like particles are about equal, as expected for random hexagonal close-packed crystal. This can be explained with the larger number of defect structures in hcp compared to fcc, as explained above. In contrast to the simulation studies of the pure crystal structures, the perfect fcc and hcp structures are rarely found in the microscopy data of small crystal nuclei, where most of the crystal-like particles are on the surface of a nucleus and have fluid-like neighbors with a local environment that is not as ordered as in the bulk crystal. This implies that most crystal-like particles have a deformed environment, and mostly deformed graph structures are found. The particles that are found to have a crystal-like graph but are not crystal-like according to the q_6 criterion, are mostly not far from a particle with crystal-like q_6: 72% of them are found to have at least one neighbor and 54% have at least two neighbors with crystal-like q_6. Therefore, the differences between the two methods concern predominantly the surfaces of crystal nuclei determined using the bond-order method.

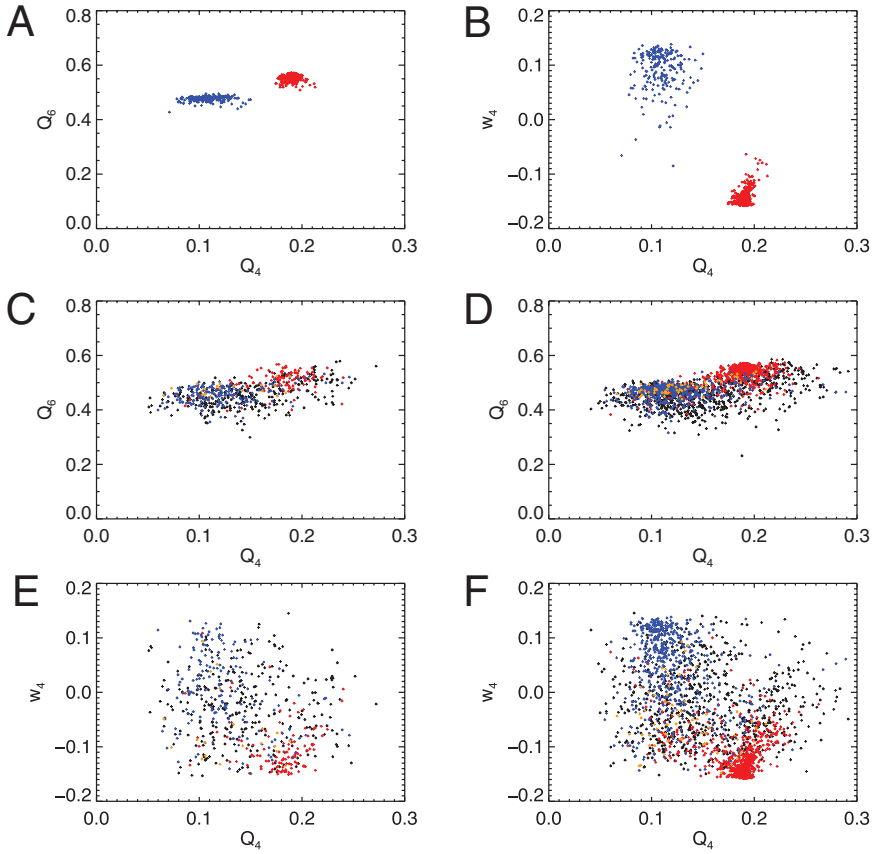

Fig. 7. Comparison of structure characterization with the graph and bond-order method for a measurement at $\phi = 0.28$. Fcc- and hcp-like particles are shown in red and blue, respectively. (A, B) Particles with perfect fcc and hcp graph-structure. (C, E) All particles one hour after shear melting the sample. (D, F) All particles 66 hours after shear melting the sample. In (C, D, E, F) orange symbols refer to undetermined crystal-like particles and black symbols to particles with unknown structure.

3.5.2 Comparison of local structure determination

The bond-order parameter and the graph method show a good agreement in the determination of fcc- and hcp-like structures. If we consider the particles with a perfect fcc or hcp graph, they are also clearly separated using the bond-order parameters, as shown in Fig. 7A and B. With all crystal particles according to the bond-order method, the agreement is still good (Fig. 7C, D, E, F): Most fcc- (red) and hcp-like (blue) particles lie in the expected range of the bond-order parameters. 3% are recognized as particles with an undetermined crystal structure and 48% have an unknown structure at the beginning of the measurement. This number decreases with time to about 35%. The unknown structures are spread out allover the fcc- and hcp-like regions in the bond-order parameter plots.

The amount of fcc- and hcp-like crystal-like particles is found to develop with time, as nucleation and crystal growth proceed and the number of crystal-like particles increases. The fraction of hcp-like particles is larger than the fcc fraction at

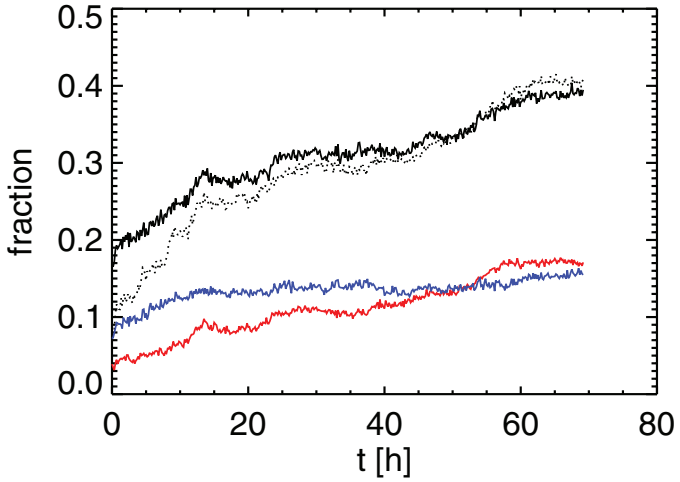

Fig. 8. Temporal evolution of the fractions of crystal-like particles determined using the graph- or the bond-order parameter method in a sample with $\phi = 0.28$: All crystal-like particles identified using the graph method (black line) and the q_6 method (dotted line), fcc-like (red) and hcp-like (blue) particles identified using the graph method. $t = 0$ is set by the time the sample was shear melted.

early times, when nucleation starts and crystal nuclei are small, as shown in Fig. 8. We interpret this as a consequence of the predominance of strongly deformed graphs that have a larger probability to correspond to a hcp-like structure. At later times, when nuclei of about critical or postcritical size contain the majority of crystal-like particles, the fraction of fcc-like particles keeps increasing and that of hcp-like particles grows slower or stays roughly constant. When crystal nuclei are sorted according to their size, the same trend is observed: With increasing nucleus size, the fraction of hcp-like particles does not grow as fast as the fraction of fcc-like particles. This is as expected, since the average nucleus size also increases with time.

4 Conclusions

Taking into account that bond-order parameters on the one hand and graphs or SP rings on the other focus on different aspects of local structures, the agreement of both methods is good. Even the detection of crystal-like particles and small crystal nuclei with the graph method is similar to that with bond-order parameters. Using the nearest neighbor structures detected in a simulation at the same volume fraction as a measurement, the graph method does not detect as many crystal-like particles, but nuclei consisting of $\gtrsim 10$ particles are detected with both methods. It follows that the graph method can serve to detect and follow crystal nuclei analogous to the bond-order parameter method. The graph method is, however, more involved, because the various graphs used for structure determination have to be collected from a reference measurement or a simulation, while the bond-order method does not need such a reference. The agreement of the volume fractions of experiment and reference is important, as the number of graph-structures depends strongly on volume fraction (Table 1).

References

1. K.F. Kelton. Crystal nucleation in liquids and glasses. In H. Ehrenbach, D. Turnbull, editors, *Solid State Physics*, volume 45, (Academic Press, Boston, 1991) p. 75
2. U Gasser. J. Phys.: Cond. Mat. **21**, 203101 (2009)
3. U. Gasser, E.R. Weeks, A. Schofield, P.N. Pusey, D.A. Weitz. Science **292**, 258 (2001)
4. Pieter Rein ten Wolde, Maria J. Ruiz-Montero, Daan Frenkel. Phys. Rev. Lett. **75**, 2714 (1995)
5. P.N. Pusey, W. van Megen. Nature **320**, 340 (1986)
6. P.N. Pusey, W. van Megen, P. Bartlett, B.J. Ackerson, J.G. Rarity, S.M. Phys. Rev. Lett. **63**, 2753 (1989)
7. K. Schaetzel, B.J. Ackerson. Phys. Rev. E **48**, 3766 (1993)
8. B.J. Ackerson, K. Schaetzel. Phys. Rev. E **52**, 6448 (1995)
9. V. Prasad, D. Semwogerere, E.R. Weeks. J. Phys.: Cond. Mat. **19**, 113102 (2007)
10. J.C. Crocker, D.G. Grier. Journal of Colloid and Interface Science **179**, 298 (1996)
11. K. Sandomirski, E. Allahyarov, H. Lowen, S.U. Egelhaaf. Soft Matter, **7**, 8050 (2011)
12. F. Ziese, G. Maret, U. Gasser. J. Phys.: Condens. Matter, **25**, 375105 (2013)
13. P.J. Steinhardt, D.R. Nelson, M. Ronchetti. Phys. Rev. B, **28**, 784 (1983)
14. J.S. van Duijneveldt, D. Frenkel. J. Chem. Phys. **96**, 4655 (1992)
15. S. Auer, D. Frenkel. J. Chem. Phys., **120**, 3015 (2004)
16. C. Desgranges, J. Delhommelle. Phys. Rev. B **77**, 6 (2008)
17. U. Gasser, A. Schofield, D.A. Weitz. J. Phys.: Condens. Matter, **15**, S375 (2003)
18. M. Leocmach, H. Tanaka. Nature Communications **3**, 8 2012
19. W. Lechner, C. Dellago. J. Chem. Phys., **129**, 5 (2008)
20. D.S. Franzblau. Phys. Rev. B, **44**, 4925 (1991)
21. S.W. Provencher. Computer Physics Communications **27**, 213 (1982)
22. A.-P. Hynninen, M. Dijkstra. Phys. Rev. E, **68**, 021407 (2003)
23. J.-P. Hansen, Ian R. McDonald. *Theory of simple liquids*, 2nd edn (Academic Press, London, 1986)
24. G. Voronoi. Journal Fur Die Reine Und Angewandte Mathematik **133**, 97 (1908)
25. J.L. Finney. Journal of Computational Physics, **32**, 137 (1979)
26. J.P. Troadec, A. Gervois, L. Oger. Europhysics Letters, **42**, 167 (1998)
27. B. O'Malley. *Molecular Dynamics Investigation of Crystallization in the Hard Sphere System*. PhD thesis (Royal Melbourne Institute of Technology, 2001)
28. W. Mickel, S.C. Kapfer, G.E. Schroder-Turk, K. Mecke. J. Chem. Phys. **138**, 7 (2013)
29. P.N. Pusey, E. Zaccarelli, C. Valeriani, E. Sanz, W.C.K. Poon, M.E. Cates. Philosophical Transactions of the Royal Society a-Mathematical Physical and Engineering Sciences, **367**, 4993 (2009)
30. S. Auer D. Frenkel. Ann. Rev. Phys. Chem. **55**, 333 (2004)
31. S. Auer D. Frenkel. Adv. Polym. Sci., **173**, 149 (2005)
32. P. Rein ten Wolde, M.J. Ruiz-Montero, D. Frenkel. J. Chem. Phys., **104**, 9932 (1996)
33. S. Auer, D. Frenkel. Nature, **413**, 711 (2001)
34. B. O'Malley, I. Snook. J. Chem. Phys. **123**, 054511 (2005)
35. Y.H. Chui, R.J. Rees, I.K. Snook, B. O'Malley, S.P. Russo. The Journal of Chemical Physics, **125**, 114703 (2006)